Journal of Groundwater Science and Engineering 13(2025) 22−33

Journal homepage: http://gwse.iheg.org.cn

Research Article

Quantitative study on vertical distribution of heat flow in Niutuozhen geothermal field, Xiong'an New Area—Evidence from heat flow determination in the Archean of D01 well

Ya-hui Yao[1,3,4], Xiao-feng Jia[1,3*], Sheng-tao Li[1,2,3], Jun-yan Cui[1,5], Hong Xiang[1,3], Dong-dong Yue[1,3], Qiu-xia Zhang[1,3], Zhao-long Feng[1,3]

[1] *Center for Hydrogeology and Environmental Geology*, *China Geological Survey*, *Tianjin* 300304, *China*.
[2] *Technology Innovation Center for Geological Environment Monitoring Engineering*, *MNR*, *Tianjin* 300304, *China*.
[3] *Tianjin Engineering Center of Geothermal Resources Exploration and Development*, *Tianjin* 300304, *China*.
[4] *School of Resource and Earth Science*, *China University of Mining and Technology*, *Xuzhou* 221116, *Jiangsu*, *China*.
[5] *Chinese Academy of Geological Sciences*, *Beijing* 100037, *China*.

Abstract: The karst geothermal reservoir in Xiong'an New Area is a representative example of an ancient buried hill geothermal system. However, published heat flow data are predominantly derived from the Cenozoic sedimentary cap. Due to the limited depth of borehole exploration, heat flow measurements and analyses of the Archean crystalline basement in the study area are rare. Further investigation of the heat flow and temperature field characteristics within the Archean crystalline basement beneath the karst geothermal reservoir is necessary to understand the vertical distribution of heat flow and improve the geothermal genetic mechanism in the area. The D01 deep geothermal scientific drilling parameter well was implemented in the Niutuozhen geothermal field of Xiong'an New Area. The well exposed the entire Gaoyuzhaung Formation karst geotheremal reservoir of the Jixian system and drilled 1,723.67 m into the Archean crystalline basement, providing the necessary conditions for determining its heat flow. This study involved borehole temperature measurements and thermophysical property testing of core samples from the D01 well to analyze the vertical distribution of heat flow. The findings revealed distinct segmentation in the geothermal gradient and rock thermophysical properties. The geothermal reservoir of Gaoyuzhuang Formation is dominated by convection, with significant temperature inversions corresponding to karst fracture developments. In contrast, the Archean crystalline basement exhibits conductive heat transfer. After 233 days of static equilibrium, the average geothermal gradients of the Gaoyuzhuang Formation and the Archean crystalline basement were determined to be 1.5°C/km and 18.3°C/km, respectively. These values adjusted to −0.8°C/km and 18.2°C/km after 551 days, with the longer static time curve approaching steady-state conditions. The average thermal conductivity of dolomite in Gaoyuzhuang Formation was measured as 4.37±0.82 W/(K·m), and that of Archean gneiss as 2.41±0.40 W/(K·m). The average radioactive heat generation rate were 0.30±0.32 μW/m^3 for dolomite and 1.32±0.69 μW/m^3 for gneiss. Using the temperature curve after 551 days and thermal conductivity data, the Archean heat flow at the D01 well was calculated as (43.9±7.0) mW/m^2, While the heat flow for the Neogene sedimentary cap was estimated at 88.6mW/m^2. The heat flow of Neogene sedimentary caprock is significantly higher than that of Archean crystalline basement at the D01 well, with an excess of 44.7 mW/m^2 accounting for approximately 50% of the total heat flow in the Neogene sedimentary caprock. This is primarily attributed to lateral thermal convection within the high-porosity and high-permeability karst dolomite layer, and vertical thermal convection facilitated by the Niudong fault, which collectively contribute to the heat supply of the Neogene sedimentary caprock. Thermal convection in karst fissure and fault zone contribute approximately 50% of the heat flow in the Neogene sedimentary caprock. This study quantitatively revealed the vertical distribution of heat flow, providing empirical evidence for the genetic mechanism of the convection-conduction geothermal system in sedimentary basins.

Keywords: Heat flow vertical difference; Archean crystalline basement; Thermal conductivity; Niutuozhen geothermal field; Present-day temperature field; Geothermal genetic mechanism; D01 well

Received: 05 Feb 2024/ Accepted: 16 Oct 2024/ Published: 10 Feb 2025

*Corresponding author: Xiao-feng Jia, *E-mail address*: jiaxiaofeng@mail.cgs.gov.cn

DOI: 10.26599/JGSE.2025.9280036

Yao YH, Jia XF, Li ST, et al. 2025. Quantitative study on vertical distribution of heat flow in Niutuozhen geothermal field, Xiong'an New Area—Evidence from heat flow determination in the Archean of D01 well. Journal of Groundwater Science and Engineering, 13(1): 22-33.

Introduction

The establishment of Xiong'an New Area in China was announced as part of measures to promote the coordinated development of the Beijing-Tianjin-Hebei region on April 1, 2017. Covering around 2,000 km^2 (Fig. 1), Xiong'an New Area is located in the hinterland of Beijing, Tianjin and Hebei and

is known for its abundant geothermal resources. Its primary reservoir is the Jixian system karst geothermal reservoir, with previous exploration and development activities concentrated at depths shallower than 1,800 m (Wu et al. 2018). At present, numerous studies have examined terrestrial heat flow in the region (Cui et al. 2019; Guo et al. 2019; Wang et al. 2021b; Wang et al. 2019ab; Guo, 2020; Hao, 2021). However, reports of heat flow measured from the Archean crystalline basement in Xiong'an New Area are scarce, mainly due to the limited depth of existing boreholes. Determining heat flow in the Archean crystalline basement is critical to understanding its heat flow and temperature field characteristics and analyzing the heat contribution of groundwater thermal convection in karst geothermal reservoir and water-flowing faults.

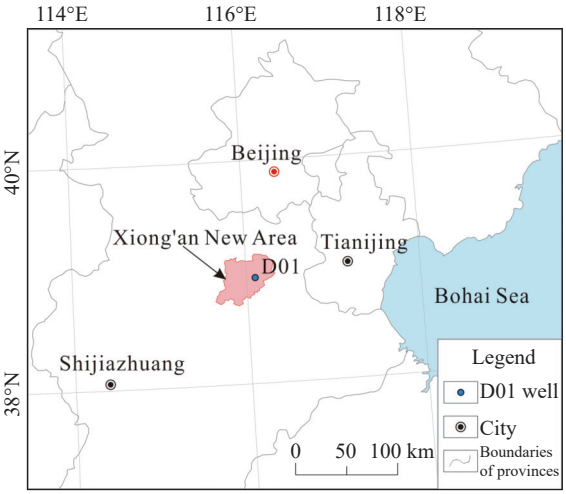

Fig. 1 Location of Xiong'an New Area and D01 Well

Previous studies indicate that the Niutuozhen geothermal field represents a typical themal convection-conduction composite geothermal system (Pang et al. 2017). Most published heat flow data in Xiong'an New Area are derived from the Cenozoic sedimentary cap. These data are influenced by groundwater thermal convection, which incorporates the convective heat contribution from the underlying karst geothermal reservoir. In contrast, heat flow and temperature field characteristics in the Archean crystalline basement beneath the karst geothermal reservoir better reflect the region's thermal background, providing a basis for lithospheric thermal structure and geodynamics analyses (Wang et al. 2022). Existing research on the geothermal genesis of the large-scale karst geothermal field in Xiong'an New Area lacks the constraints provided by background heat flow values from the Archean crystalline basement. Furthermore, discussions of the factors influencing the spatial distribution of heat flow are often limited to qualitative inference. This necessitates further investigation to enhance understanding of the geothermal genesis mechanism in the study area.

Heat flow, or terrestrial heat flow, is the most direct representation of thermal process within earth's interior and contains rich geological information. Measuring, compiling, and analyzing heat flow are fundamental to geothermal research. At present 2,337 heat flow data points from mainland China have been published in five editions (Wang et al. 2024), forming a valuable dataset for lithospheric dynamics research and geothermal resource evaluation. Historically, heat flow was thought to reflect heat transmitted by steady state heat conduction alone. However, in unsteady or convection states, Earth's heat dissipation is represented by heat flux, encompassing both conduction and convection components (Furlong and Chapman, 2013). The second edition of Geophysical Terminology revised the definition of terrestrial heat flow to include both conduction and convection components (He and Wang, 2021). Within Xiong'an New Area and its surrounding areas, the heat flow data from the Archean crystalline basement are sparse. The first edition of the heat flow data compilation for mainland China included three values (Wang and Huang, 1988), the fourth and fifth edition incorporated 10 values and 53 values, respectively. (Jiang et al. 2016; Wang et al. 2024). These values were primarily measured from the dolomite of Proterozoic Jixian system and the Neogene sedimentary strata.

Since 2018, the China Geological Survey has implemented several deep geothermal parameter wells, such as D16 and D17, in Xiong'an New Area to support the geothermal resource planning and expand reservoir exploration (Sun et al. 2023; Wang et al. 2020; Wang et al. 2018a). Notably, the D01 well in the Niutuozhen geothermal field, with a completed drilling depth of 3,403.67 m, penetrates the karst geothermal reservoir of the Gaoyuzhuang Formation of Jixian system and exposes a 1,723.67 m section of the Archean crystalline basement. This provides a unique opportunity to study the temperature characteristics of deep karst geothermal reservoir and Archean crystalline basements (Yao et al. 2022).

1 Geological setting

Xiong'an New Area is located within the Jizhong Depression, a secondary structural unit of Bohai Bay Basin. It can be divided into structural

subunits, including the Rongcheng Uplift in the northwest, the Niutuozhen Uplift in the northeast, and the Gaoyang Uplift in the south (Fig. 2). The Niutuozhen Uplift is bounded by the Niudong Fault, Niunan Fault, Rongcheng Fault and Daxing Fault. The primary stratigraphic sequence, from bottom to top, comprises the Archaeozoic basement, Changcheng system, Jixian system, Paleogene, Neogene and Quaternary formations. Previous studies (Chen et al. 1982; Li et al. 2014; Pang et al. 2017; Pang et al. 2020) indicate that the geothermal anomaly in Niutuozhen Uplift was formed within a typical geothermal background. Under the structural configuration of concave and convex features, as the bedrock's higher thermal conductivity compared to the sedimentary caprock redistributes heat flow, concentrating it in the uplifted area with high conductivity. This results in morate-to-high heat flow in these regions, with heat source predominantly originating from mantle heat flow and radiogenic heat generation within the crust (Wang, 2022; Wang et al. 2021a). Fault structures within the uplift promote karstification of carbonate rocks, thereby creating reservoir spaces and seepage channels for karst geothermal reservoirs (Wang et al. 2018b; Wang et al. 2022; Xing et al. 2022).

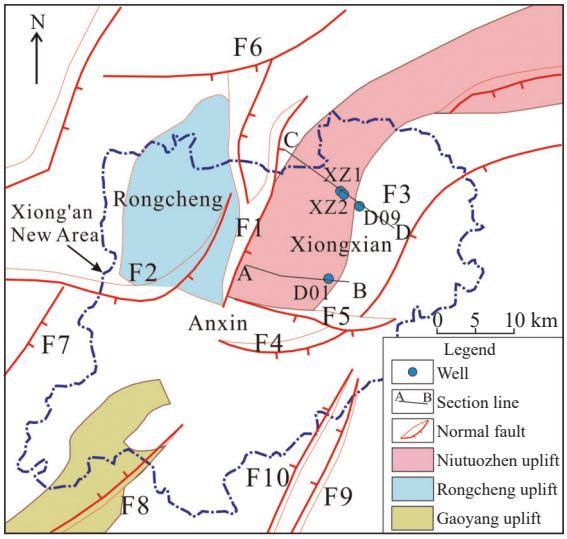

Fig. 2 Tectonic units and major fault distribution in the study area

(F1: Rongcheng fault, F2: Xushui fault, F3: Niudong fault, F4: Anxin south fault, F5: Niunan fault, F6: Daxing fault, F7: Baoding-Shijiazhuang fault, F8: Gaoyang-Boye fault, F9: Renqiu fault, F10: Renxi fault). (Adapted from Dai et al. 2019)

The geothermal water within the karst geothermal reservoir is primarily replenished through lateral migration from the Taihang Mountain to the west and the Yanshan Mountains to the north. This water undergoes deep circulation heating before stored within the reservoir. Karst fissures form the main channels for lateral geothermal water movement, while fault structures act as vertical conduits for geothermal water migration from deep to shallow depths.

D01 Well is located in the southeastern region of Xiongxian County, Xiong'an New Area, positioned in the southeastern part of the Niutuozhen Uplift and approximately 800 m east of the rear edge of the Niudong Fault (Fig. 2). During drilling, the formations encountered included Quaternary clay and sandy clay, siltstone and mudstone of Neogene, glutenite of Neogene Guantao Formation, dolomite of Gaoyuzhuang Formation, and Archaean gneiss (Fig. 3). The Gaoyuzhuang Formation in D01 Well demonstrates excellent geothermal reservoir properties, with a water inflow rate of 119.3 m^3/h and a water outlet temperature of 64°C, Indicating its high water abundance and geothermal resource potential.

2 Borehole temperature measurement

Borehole temperature measurement is a fundamental approach to determine heat flow values and analyze subsurface temperature fields. It also plays a crucial role in evaluating deep geothermal resources. This technique uses the well fluid as a medium to indirectly measure the formation temperature of the well wall. However, the drilling process, comprising the lifting and rotation of drilling tools, fluid circulation, and potential fluid leakage, can alter the temperature of the well fluid and surrounding formation. These disturbances introduce discrepancies between the measured well temperatures and the true formation temperatures. Following the completion of drilling, the measured temperatures may vary depending on the static well time (He et al. 2008).

In this study, borehole temperature measurements for D01 Well were conducted on December 18, 2019 and October 31, 2020. The time intervals between the cessation of drilling and the two temperature measurements were 233 days and 551 days, respectively. The measurements utilized a PPS71 high-temperature storage logging tool, which offers an accuracy of ± 3%, a range of 0–350°C, and a resolution of 0.01°C. The extended static well time ensured that the well fluid temperature closely approximated the true formation temperature, indicating that the thermal system had largely stabilized. The temperature measurement curves for D01 Well (Fig. 4) reveal clear segmentation. The Neogene and Archean sections exhibit

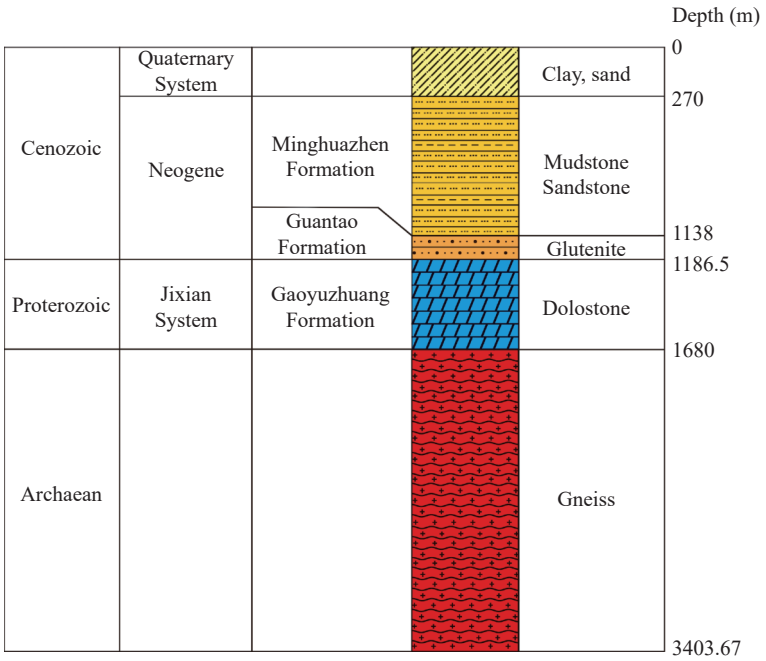

Fig. 3 Stratigraphic histogram of D01 well

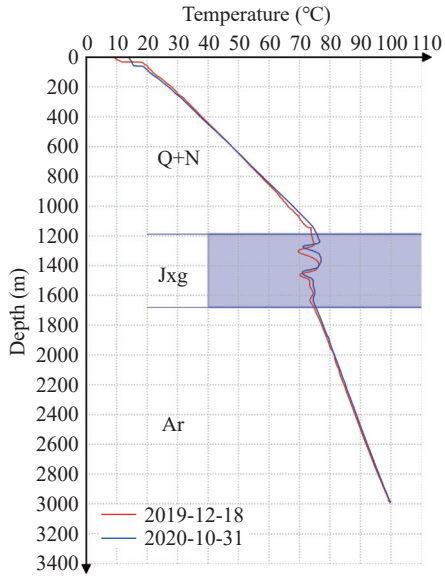

Fig. 4 Temperature curve of D01 well in near steady state

distinct conductive geothermal characteristics. In contrast, the geothermal reservoir within the Gaoyuzhuang Formation shows relatively uniform temperatures. The average geothermal gradients within the Gaoyuzhuang Formation were calculated as 1.5°C/km and −0.8°C/km for static well times of 233 days and 551 days, respectively, reflecting pronounced convective geothermal characteristics. Additionally, the temperature curves display temperature inversions within fracture-rich zone of the Gaoyuzhuang Formation, indicating the effects of thermal convection driven by fluid movement within these karst fissures.

To account for the influence of near-surface temperature and the convection section of the karst geothermal reservoir of the Gaoyuzhuang Formation, the 400–800 m depth section of the Neogene sedimentary caprock was selected for the geothermal gradient measurement. Similarly, considering that the Archean geothermal temperature is partially affected by the convection section of the Gaoyuzhuang Formation, the 2,300–2,700 m depth section was selected for the Archean geothermal gradient measurement. The temperature measurement data of these selected depth sections in the Neogene sedimentary caprock and Archaean formations were subjected to linearly fitting. The fitting results for a static time of 233 days are shown in Fig. 5 (a) and Fig. 5 (b), yielding the following fitting formulas for temperature T (°C) and depth H (m) for Neogene and the Archean formations:

$$T = 0.0486H + 18.228 \qquad R^2 = 0.99978 \qquad (1)$$

$$T = 0.0183H + 44.091 \qquad R^2 = 0.99986 \qquad (2)$$

For a static time of 551 days, the linear fitting results are presented in Fig. 5 (c) and Fig. 5 (d), with the corresponding fitting formulas:

$$T = 0.0509H + 17.222 \qquad R^2 = 0.99975 \qquad (3)$$

$$T = 0.0182H + 45.077 \qquad R^2 = 0.99983 \qquad (4)$$

Based on these fitting formulas, the average geothermal gradients for the Neogene and Archaean formations were determined to be 48.6°C/km

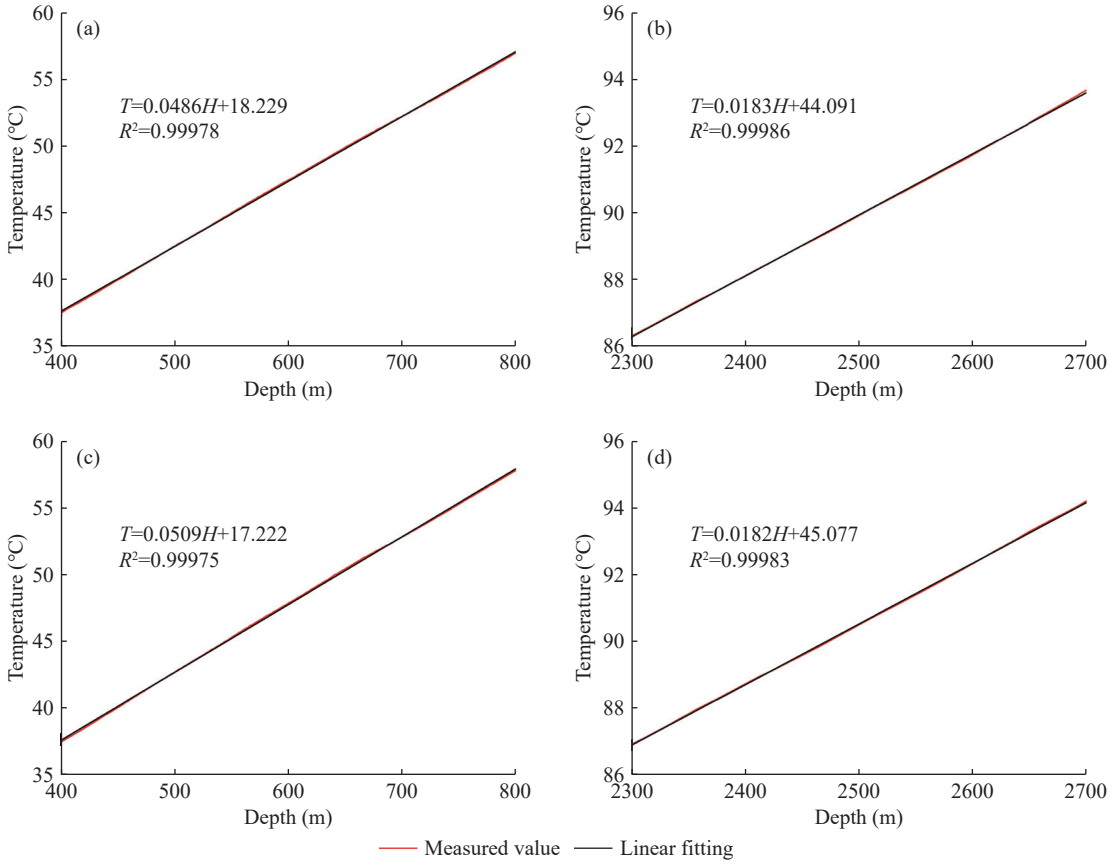

Fig. 5 Linear fitting of temperature measurement data for Neogene and Archean heat flow calculation sections

and 18.3°C/km, respectively, for the 233-day static period. For the 551-day static period, the average geothermal gradients were calculated as 50.9°C/km and 18.2°C/km, respectively.

3 Heat flow determination

3.1 Thermal conductivity

The thermal conductivity of rocks is influenced by various factors, including mineral composition, porosity, water saturation, pressure, temperature and other factors (Norden et al. 2020; Pribnow et al. 1996). For Archean gneiss core samples, which are characterized by compact structure and low porosity, the effects of pressure on thermal conductivity, which is calculated using the pressure correction formula (Seipold and Huenges, 1998), are less than 1%. As a result, pressure and saturation corrections are disregarded, and only temperature correction is applied to thermal conductivity. The following temperature correction formulas (Sass et al. 1992) were applied to the measured thermal conductivity values of Archean gneiss.

$$\lambda(0) = \lambda(25)\{1.007 + 25[0.0037 - 0.0074/\lambda(25)]\} \quad (5)$$

$$\lambda(T) = \lambda(0)/\{1.007 + T[0.0036 - 0.0072/\lambda(0)]\} \quad (6)$$

Where: λ (0) and λ (25) are measured thermal conductivity at 0°C and 25°C, W/(K·m); λ (25) is the thermal conductivity test value; T is the in-situ temperature of rock,°C; λ (T) is the in-situ thermal conductivity of rock at temperature T.

A total of 25 gneiss core samples were collected from depths of 2,300–2,700 m in the Archean strata of the D01 well for thermal conductivity testing. Two types of equipment were used for the comparative analysis. One is the Hot Disk (TPS 1500) thermal constant analyzer made in Sweden. The measurement principle is the transient plane heat source method. The test accuracy is ± 2%, and the measurement range is 0.03–500W/(K·m). The other equipment used is the TC 3200 thermal conductivity instrument made in China and the measurement principle is the transient hot wire method. The measurement accuracy is ± 5%, and the measurement range is 0.001–20 W/(K·m). The thermal conductivity values obtained by the two methods for the same sample were closely aligned, confirming the reliability of the data. The average measured values from both methods were used for heat flow calculations, with temperature correction applied. After correction, the thermal conductivity of the Archean gneiss core ranged from 2.05

Table 1 Thermal conductivity of Archean gneiss core samples in D01 well

Depth (m)	Number of samples	Test value of thermal conductivity at room temperature (W/(K·m))			Temperature at different depths (°C)	Thermal conductivity correction value according to temperature (W/(K·m))
		Transient plane heat source method	Transient hot wire method	Average value of two methods		
2,355.47–2,356.47	4	3.15	3.26	3.20	87.4	2.94
2,445.65–2,447.85	8	2.07	2.06	2.07	89.1	2.05
2,533.56–2,536.26	12	2.94	2.91	2.92	90.7	2.71
2,581.76–2,584.46	14	2.24	2.20	2.22	91.5	2.16
2,603.58–2,605.58	12	2.29	2.25	2.27	91.9	2.20

W/(K·m) to 2.94 W/(K·m), with an average value of (2.41 ± 0.40) W/(K·m).

Since no Neogene core samples were obtained from D01 well, a reference thermal conductivity value of 1.74 W/(K·m) was adopted, based on data from the Jizhong depression and other areas of Bohai Bay Basin (Wang et al. 2019b). The average thermal conductivity of dolomite in Gaoyuzhuang Formation was determined from six core samples obtained from the D01 well. The measured value was (4.37±0.82) W/(K·m).

3.2 Radiogenic heat production

Radiogenic heat production in the Earth's crust predominantly originates from the radioactive decay of uranium (^{238}U), thorium (^{232}Th) and potassium (^{40}K), contributing approximately 98% of geothermal radiogenic heat (Wollenberg and Smith, 1987). In this study, a total of 19 core samples from the D01 well were analyzed for radiogenic heat production, including the concentration measurements of uranium, thorium and potassium. Concentrations of uranium and thorium were measured using Inductively Coupled Plasma Mass Spectrometry (ICP-MS), and the potassium concentrations were determined via atomic absorption spectroscopy. The density was measured in the lab for each sample. The radiogenic heat production was calculated using the following empirical formula (Rybach, 1988):

$$A = 10^{-5}\rho(9.52C_{\mathrm{U}} + 2.56C_{\mathrm{Th}} + 3.48C_{\mathrm{K}}) \quad (7)$$

Where: A is the heat production (μW/m^3), ρ is density (kg/m^3). C_U and C_{Th} are concentrations of U and Th in ppm, respectively, and C_K is the content of K in percentage.

The radiogenic heat production values for the core samples from the D01 well are summarized in Table 2. The average radioactive heat production rate of 6 dolomite cores in Gaoyuzhuang Formation and 13 Archean gneiss cores are (0.30±0.32) μW/m^3 and (1.32±0.69) μW/m^3.

3.3 Heat flow

Heat flow, a key parameter in geothermal studies, is typically determined indirectly using temperature measurement and rock thermal conductivity data. The calculation of heat flow is based on Fourier law of one-dimensional steady heat conduction, which can be calculated as:

$$q = -\lambda\frac{\mathrm{d}T}{\mathrm{d}Z} \quad (8)$$

Where: dT/dZ is the geothermal gradient (°C/km), λ is the rock thermal conductivity (W/(K·m)), and the negative sign indicates that the direction of heat conduction flows in the direction opposite to the geothermal gradient. To compare and analyze heat flow difference in the Xiong'an New Area, heat flow measurements were conducted for both the Neogene sedimentary caprock and the Archean crystalline basement using data from the D01 Well. Table 3 summarizes the measured heat flow values for the two geological formations.

4 Results and discussion

4.1 Heat flow vertical difference of D01 well

Based on the temperature measurement curve for a static time of 551 days and thermal conductivity data of Archean gneiss in the D01 well, the calculated heat flow from the Archean layer was (43.9±7.0) mW/m^2, while the heat flow from the Neogene sedimentary caprock was estimated at 88.6 mW/m^2. As shown in Fig. 7, the total surface heat flow q (88.6 mW/m^2) equals the sum of the conduction heat flow q_0 (43.9 mW/m^2) originating from the Archaean crystalline basement and the convection heat flow contribution q_1 (44.7 mW/m^2) from the karst geothermal reservoir. This demonstrates that thermal convection in the karst fissures and fault zones accounts for approximately 50% of

Table 2 Radiogenic heat production values for core samples from the D01 well

Sample number	Depth(m)	ρ (kg/m^3)	C_U (μg/g)	C_{Th} (μg/g)	C_K (%)	Radiogenic heat production (μW/m^3)	Lithology
1	1,185.98	2,810.3	0.071	0.421	0.459	0.09	Dolomite
2	1,191.335	2,814.6	0.278	0.7	0.642	0.19	Dolomite
3	1,322.64	2,756.1	0.247	0.521	0.22	0.12	Dolomite
4	1,401.445	2,711.5	0.143	0.372	0.08	0.07	Dolomite
5	1,500.68	2,763.4	0.597	2.33	0.683	0.39	Dolomite
6	1,498.93	2,745.1	1.57	5.54	1.17	0.91	Dolomite
7	1,717.24	2,801.7	3.01	5.86	0.214	1.24	Gneiss
8	1,915	2,843.7	2.77	6.16	0.142	1.21	Gneiss
9	2,017.83	2,834.1	3.59	0.631	2.86	1.30	Gneiss
10	2,144.2	2,934.1	2.06	6.51	1.44	1.21	Gneiss
11	2,237.73	2,853.7	4.8	9.86	11.3	3.15	Gneiss
12	2,355.97	2,689.3	6.72	2.47	0.835	1.97	Gneiss
13	2,446.75	2,853.1	1.42	12.8	3.28	1.65	Gneiss
14	2,534.905	2,859.4	1.66	0.476	0.511	0.54	Gneiss
15	2,581.96	2,897.3	2.2	0.013	0.381	0.65	Gneiss
16	2,604.38	2,853.4	2.9	2.31	0.694	1.03	Gneiss
17	2,725	2,893.1	1.45	1.07	1.38	0.62	Gneiss
18	2,817.87	2,836.7	3.53	0.548	0.867	1.08	Gneiss
19	2,893.52	2,854.3	3.52	5.32	1.94	1.54	Gneiss

Table 3 Heat flow of the Neogene and Archean formations from the D01 well

Stratum	Depth (m)	Average value of heat flow (mW/m^2)	
		233 days after the cessation of drilling	551 daysafter the cessation of drilling
N	400–800	84.6	88.6
Ar	2,300–2,700	44.1	43.9

the heat in the Neogene sedimentary caprock.

The results clearly indicate that the heat flow in the Neogene sedimentary caprock is significantly higher than that of Archean crystalline basement in the D01 well. This discrepancy can be attributed to lateral groundwater convection in the highly porous and permeable karst dolomite layer, combined with vertical convection through the Niudong fault, which transfers heat to the base of the Neogene sedimentary caprock. Furthermore, radiogenic heat production tests suggest that the contribution of radioactive heat generation between 400–2,700 m in the D01 Well is only 2.6 mW/m^2, highlighting its relatively minor role in the overall heat flow.

4.2 Other evidence of thermal convection

The vertical heat flow difference measured between the Cenozoic sedimentary cap and the Archean crystalline basement in the D01 well provides clear evidence of thermal convection within the karst geothermal reservoir. Additional supporting evidence for the thermal convection was obtained from data collected from wells D09, XZ1, and XZ2, located approximately 10km north of D01 well within the Niudong fault zone. These three wells are located relatively close to each other, with a maximum distance of around 3 km, as shown in Fig. 2. The drilling depths of the D09, XZ1, and XZ2 wells are 1,653.2 m, 1,407.9 m, and 1,282.6 m, respectively. These wells intersect the Wumishan Formation of the Jixian system at depths of 1,015 m, 893.5 m, and 778 m, respectively, with thicknesses ranging from 504.6 m to 638.2 m, although not completely exposed, as shown in Fig. 6 and Table 4. Geophysical profiles (Wang et al. 2023b) enabled predictions of the bottom depths of the karst geothermal reservoirs, corresponding to the top interfaces of the Archean, as shown in Fig. 7. Temperature curves for the three wells revealed geothermal gradients in the Cenozoic cap of 49.3°C/km, 62.4°C/km, and

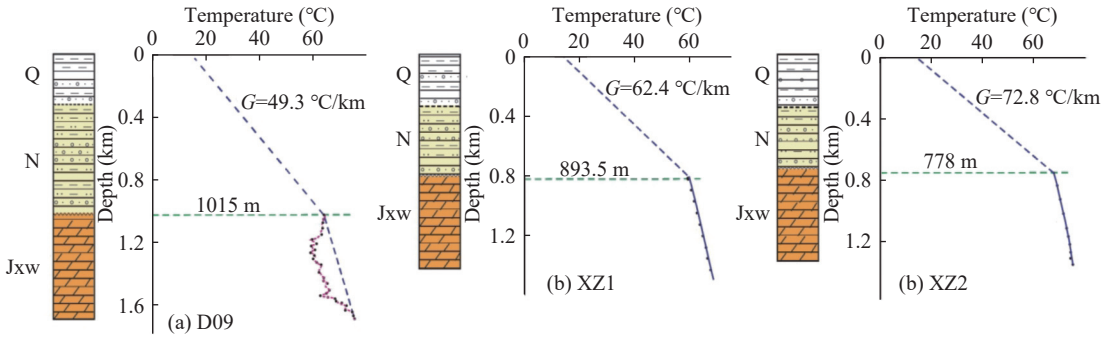

Fig. 6 Temperature curves of D09, XZ1 and XZ2 wells located within Niudong fault zone (adapted from Wang et al. 2023b)

Table 4 Burial depth of karst reservoir roof, geothermal gradient and heat flow of the Cenozoic sedimentary cap in the three wells within Niudong fault zone

Well	Depth of well (m)	Burial depth of karst reservoir roof (m)	Geothermal gradient of the Cenozoic sedimentary cap (°C/km)	Rock thermal conductivity of of the Cenozoic sedimentary cap (W/(K·m))	Heat flow of the Cenozoic sedimentary cap (mW/m^2)
D09	1,653.2	1,015	49.3	1.74	85.8
XZ1	1,407.9	893.5	62.4	1.74	108.6
XZ2	1,282.6	778	72.8	1.74	126.7

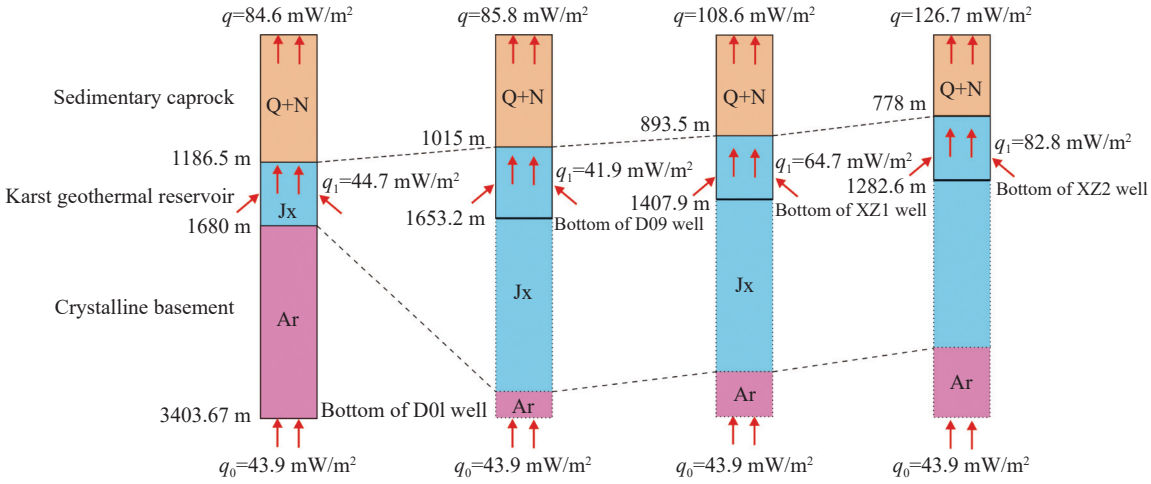

Fig. 7 The vertical heat flow difference and relationship in D01, D09, XZ1 and XZ2 well

72.8°C/km, respectively. A comparison of these gradients with the burial depth of the karst reservoir roofs (1015 m, 893.5 m, and 778 m, respectively) indicated that the shallower the burial depth correspond to higher geothermal gradients and greater heat flow in the Cenozoic caprock.

The temperature curves for the four wells discussed in this paper exhibit a significantly lower geothermal gradient within the karst reservoir sections. This trend is especially pronounced in the D01 well, where the average geothermal gradient in the Gaoyuzhuang Formation were 1.5°C/km and −0.8°C/km for static times of 233 days and 551 days, respectively, clearly demonstrating the influence of convective geothermal heat transfer. the proximity of the D09, XZ1, and XZ2 wells supports the conclusion that the Wumishan Formation reservoirs in these wells are horizontally connected.

The influence of strong groundwater convection, especially near the weathered zones at the karst reservoir interfaces, leads to overall temperature uniformity. This uniform temperature results in higher temperatures in areas where the karst reservoirs are more shallowly buried, which heats the sedimentary cover of the Cenozoic era. Consequently, the geothermal gradient in the sedimentary cover is elevated, creating a pattern where

shallower burial depths correspond to higher heat flow.

Due to the lack of exposure of the Archean crystalline basement in the D09, XZ1, and XZ2 wells, accurate heat flow values of the Archean cannot be directly obtained. However, using the measured heat flow values of the Archean crystalline basement of D01 well as a reference, the thermal convection contributions to heat flow in the D09, XZ1, and XZ2 wells were calculated to be 41.9 mW/m^2, 64.7 mW/m^2, and 82.8 mW/m^2, respectively. These values account for 48.83%, 59.58%, and 65.35% of the total heat flow in the Cenozoic cap, as shown in Fig. 7.

4.3 Geothermal geological conceptual model

Previous studies have identified the Niutuozhen geothermal field as following a "dual heat accumulation" genetic model (Pang et al. 2020). Within this model, the Niudong Fault on the eastern side of the Niutuozhen uplift is both thermal-conductive and water-conductive. Geothermal geological profiles (Fig. 8) show that high-permeability dolomite geothermal reservoir have developed in the Jixian and Changcheng systems, with the Niudong Fault serving as a conduit for groundwater migration. While permeable rock strata within the geothermal reservoir facilitate lateral groundwater migration, the faults control vertical groundwater movement.

The comparison of Neogene and Archean heat flow data from the D01 well and earlier studies provides additional insights. The analysis highlights the development of karst fissures and the presence of significant water volumes in the dolomite of the Gaoyuzhuang Formation of the D01 well. These features, combined with groundwater heat convection through the Niudong Fault, facilitate the transfer of heat from deeper strata to shallower levels. This process heats the base of Neogene sedimentary caprock, accounting for its elevated heat flow values, as shown in Fig. 7. The measured Archean heat flow beneath the karst geothermal reservoir in the D01 well also supports the heat accumulation model driven by groundwater migration and thermal-conductive and water-conductive faults.

A similar geothermal mechanism is evident in other areas of the North China Plain, such as the Xian County and Gaoyang geothermal fields, where karst geothermal reservoirs of the Wumishan and Gaoyuzhuang Formations of Jixian System are well-developed. In these areas, the geothermal genetic mechanism parallels that of the Niutuozhen geothermal field in Xiong'an New Area (Liu et al. 2022; Wang et al. 2023a). Numerical simulations, including 2D finite element modelling of coupled temperature and hydrodynamic fields, reveal that significant thermal anomalies in the Gaoyang Uplift and Xian County Uplift are primarily caused by free convection within the karst reservoir and the fault zones. These effects far outweigh the secondary influence of heat refraction due to basement fluctuation (Rao et al. 2024).

5 Conclusions

This study explored the characteristics of heat flow

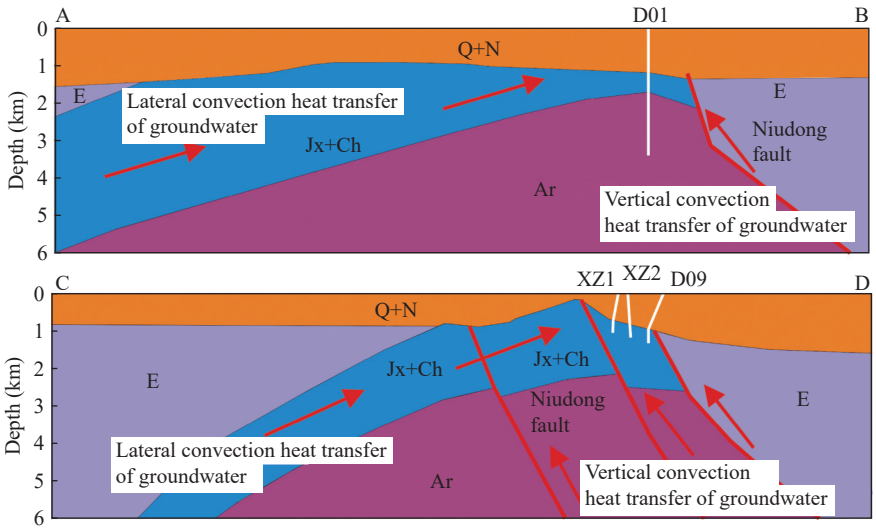

Fig. 8 The geothermal geological conceptual model of Niutuozhen Uplift (adapted from Wang et al. 2018a; Yao et al. 2022; Wang et al. 2023b)

and the present-day temperature field in the Archean crystalline basement beneath the karst geothermal reservoir of the D01 well. By conducting borehole temperature measurements and thermophysical property tests on core samples, the vertical distribution of heat flow was quantitatively analyzed. These findings provide key measured data to support the understanding of the genetic mechanism of convection-conduction type geothermal systems in sedimentary basins.

(1) Geothermal characteristics: The Neogene sedimentary caprock and Archean crystalline basement exhibit significant geothermal characteristics of conduction type, whereas the karst geothermal reservoir in the Gaoyuzhuang Formation demonstrates convection type behavior. Strong convection activity was observed in the karst geothermal reservoir section of the Gaoyuzhuang Formation in D01 well, as evidenced by temperature inversion in fracture development zones on temperature measurement curves.

(2) Heat flow comparison: The heat flow of Neogene sedimentary caprock is significantly higher than that of the Archean crystalline basement in the D01 well. This discrepancy is primarily due to the lateral thermal convection of groundwater within the high permeability karst dolomite layer and the vertical thermal convection along the Niudong Fault, which collectively heat the base of the Neogene sedimentary caprock. Approximately 50% of the heat in the Neogene sedimentary caprock can be contributed to thermal convection within the karst fissure and fault zones. The quantitative heat flow distribution in D01 well highlights that the pronounced thermal anomalies in the Niutuozhen geothermal field result from convection in the karst reservoir and the fault zones.

(3) Evidence of thermal convection: The vertical heat flow distribution, measured in the Cenozoic sedimentary cap and Archean crystalline basement, confirms the significant role of thermal convection in the karst geothermal reservoir of D01 well. A clear relationship was identified: As the burial depth of the karst reservoir roof decreases, the geothermal gradient of the Cenozoic caprock increases, leading to elevated heat flow in the Cenozoic cap. Under the strong influence of groundwater thermal convection, especially in the weathering shell stage of the karst reservoir section, the overall temperature becomes uniform. This results in high temperatures in areas with shallow burial depth of the karst reservoir, heating up the Cenozoic sedimentary cover and creating a higher geothermal gradient in these areas. Consequently, regions with shallower burial depths of the karst geothermal reservoir exhibit locally higher heat flow.

Acknowledgement

The research was funded by the National Key Research and Development Program (Grant Nos. 2021YFB1507404 and 2018YFC0604305) and the Project of China Geological Survey (Grant Nos. DD20221680, DD20189113, and DD20190127).

References

Chen MX, Huang GS, Zhang WR, et al. 1982. The temperature distribution pattern and the utilization of geothermal water at Niutuozhen basement protrusion of central Hebei province. Chinese Journal of Geology, 17(3): 239−252. (in Chinese)

Cui Y, Zhu CQ, Qiu NS, et al. 2019. Radioactive heat production and terrestrial heat flow in the Xiong'an Area, North China. Energies, 12(24): 4608. DOI：10.3390/en12244608.

Dai MG, Lei HF, Hu JG, et al. 2019. Evaluation of recoverable geothermal resources and development parameters of Mesoproterozoic thermal reservoir with the top surface depth of 3500m and shallow in Xiong'an New Area. Acta Geologica Sinica, 93(11): 2874−2888. (in Chinese) DOI：10.19762/j.cnki.dizhixuebao.2019200.

Furlong KP, Chapman DS. 2013. Heat flow, heat generation, and the thermal state of the lithosphere. Annual Review of Earth and Planetary Sciences, 41(1): 385−410. DOI：10.1146/annurev.earth.031208.100051.

Guo SS, Zhu CQ, Qiu NS, et al. 2019. Present Geothermal Characteristics and Influencing Factors in the Xiong'an New Area, North China. Energies, 12(20). DOI：10.3390/en12203884.

Guo SS. 2020. Present geothermal characteristics and its influencing factors in Xiong'an New Area. M. S. thesis. Beijing: China University of Petroleum: 54−58. (in Chinese) DOI：10.27643/d.cnki.gsybu.2020.001411.

Hao ZJ. 2021. Geothermal field characteristics and influencing factors of Niutuozhen Uplift area in Jizhong Depression. M. S. thesis. Beijing: China University of Petroleum: 44−52. (in

Chinese) DOI：10.27643/d.cnki.gsybu.2021.001474.

He LJ, Hu SB, Huang SP, et al. 2008. Heat flow study at the Chinese Continental Scientific Drilling site: Borehole temperature, thermal conductivity, and radiogenic heat production. Journal of Geophysics Research, 113(B2). DOI：10.1029/2007JB004958.

He LJ, Wang JY. 2021. Concept and application of some important terms in Geothermics and Geophysics such as terrestrial heat flow. China Terminology, 23(03): 3−9. (in Chinese) DOI：10.12339/j.issn.1673-8578.2021.03.001.

Jiang GZ, Gao P, Rao S, et al. 2016. Compilation of heat flow data in the continental area of China (4th edition). Chinese Journal of Geophysics, 59(8): 2892−2910. (in Chinese) DOI：10.6038/cjg20160815.

Li WW, Rao S, Tang XY, et al. 2014. Borehole temperature logging and temperature field in the Xiongxian geothermal field, Hebei Province. Chinese Journal of Geology, 49(03): 850−863. (in Chinese) DOI：10.3969/j.issn.0563-5020.2014.03.012.

Liu YG, Long XT, Liu F. 2022. Tracer test and design optimization of doublet system of carbonate geothermal reservoirs. Geothermics, 105: 102533. DOI：10.1016/j.geothermics.2022.102533.

Norden B, Förster A, Förster H, et al. 2020. Temperature and pressure corrections applied to rock thermal conductivity: Impact on subsurface temperature prognosis and heat-flow determination in geothermal exploration. Geothermal energy (Heidelberg), 8(1): 1−19. DOI：10.1186/s40517-020-0157-0.

Pang ZH, Kong YL, Pang JM, et al. 2017. Geothermal resources and development in Xiong'an New Area. Bulletin of Chinese Academy of Sciences, 32(11): 1224−1230. (in Chinese) DOI：10.16418/j.issn.1000-3045.2017.11.007.

Pang ZH, Pang JM, Kong YL, et al. 2020. Large-scale karst thermal storage identification method and large-scale sustainable mining technology. Science and Technology for Development, 16(Z1): 299−306. (in Chinese) DOI：10.11842/chips.20200516001.

Pribnow D, Williams CF, Sass JH, et al. 1996. Thermal conductivity of water-saturated rocks from the KTB Pilot Hole at temperatures of 25 to 300°C. Geophysical Research Letters, 23(4): 391−394. DOI：10.1029/95GL00253.

Rao S, Luo Y, Huang SD, et al. 2024. Heat accumulation effect of groundwater convective activity in karst geotherma reservoir in Jizhong Depression, Bohai Bay Basin. Chinese Journal of Geophysics, 67(08): 3075−3088. (in Chinese) DOI：10.6038/cig2024S0016.

Rybach L. 1988. Determination of heat production rate, in handbook of terrestrial heat flow density determination, edited by R. Haenel et al. Kluwer Acad., Dordrecht, Netherlands: 125−142.

Sass JH, Lachenbruch AH, Moses TH, et al. 1992. Heat flow from a scientific research well at Cajon Pass, California. Journal of Geophysical Research, 97(B4): 5017−5030. DOI：10.1029/91JB01504.

Seipold U, Huenges E. 1998. Thermal properties of gneisses and amphibolites — high pressure and high temperature investigations of KTB-rock samples. Tectonophysics, 291(1): 173−178. DOI:10.1016/S0040-1951(98)00038-9

Sun JX, Yue GF, Zhang W. 2023. Simulation of thermal breakthrough factors affecting carbonate geothermal-to-well systems. Journal of Groundwater Science and Engineering, 11(4): 379−390. DOI：10.26599/JGSE.2023.9280030.

Wang GL, Li J, Wu AM, et al. 2018a. A study of the thermal storage characteristics of Gaoyuzhuang Formation, A new layer system of thermal reservoir in Rongcheng uplift area, Hebei province. Acta Geoscientica Sinica, 39(05): 533−541. (in Chinese) DOI：10.3975/cagsb.2018.071901.

Wang GL, Liu YG, Duan HX, et al. 2023a. Crust-mantle differentiation and thermal accumulation mechanisms in the north China plain. Renewable Energy, 213: 63−74. DOI：10.1016/j.renene.2023.05.136.

Wang GL, Wang WL, Zhang W, et al. 2020. The status quo and prospect of geothermal resources exploration and development in Beijing-Tianjin-Hebei region in China. China Geology, 3(1): 173−181. DOI：10.31035/

cg2020013.

Wang JY, Huang SP. 1988. Compilation of heat flow data in the China Continental area. Chinese Journal of Geology (Scientia Geologica Sinica), 23(2): 196−204. (in Chinese)

Wang K, Zhang J, Bai DW, et al. 2021a. Geothermal-geological model of Xiong'an New Area: Evidence from geophysics. Geology in China, 48(05): 1453−1468. (in Chinese) DOI：10.12029/gc20210511.

Wang K. 2022. Study on the geothermal geological structure and deep geothermal source mechanism of Xiong'an New Area based on comprehensive geophysical exploration. Ph. D. thesis. Chang Chun: Jilin University: 117−122. (in Chinese) DOI：10.27162/d.cnki.gjlin.2022.007525.

Wang SF, Liu JR, Sun Y, et al. 2018b. Study on the geothermal production and reinjection mode in Xiong County. Journal of Groundwater Science and Engineering, 6(3): 178−186. DOI：10.19637/j.cnki.2305-7068.2018.03.003.

Wang XW, Guo SY, Gao NA, et al. 2023b. Detection of carbonate geothermal reservoir in Niudong fault zone of Xiong'an New Area and its geothermal exploration significance. Geological Bulletin of China, 42(1): 14−26. (in Chinese) DOI：10.12097/j.issn.1671-2552.2023.01.002.

Wang ZT, Gao P, Jiang GZ, et al. 2021b. Heat flow correction for the high-permeability formation: A Case Study for Xiong'an New Area. Lithosphere, 2021(Special 5). DOI: 10.2113/2021/9171191

Wang ZT, Hu SB, Wang YB, et al. 2022. Influence of the groundwater convection within the high permeability formation on the overlying temperature field in Niutuozhen uplift. Chinese Journal of Geophysics, 65(2): 726−736. (in Chinese) DOI：10.6038/cjg2022P0341.

Wang ZT, Jiang GZ, Zhang C, et al. 2019a. Thermal regime of the lithosphere and geothermal potential in Xiong'an New Area. Energy Exploration & Exploitation, 37(2): 787−810. DOI：10.1177/0144598718778163.

Wang ZT, Zhang C, Jiang GZ, et al. 2019b. Present-day geothermal field of Xiong'an New Area and its heat source mechanism. Chinese Journal of Geophysics, 62(11): 4313−4322. (in Chinese) DOI：10.6038/cig2019M0326.

Wollenberg HA, Smith AR. 1987. Radiogenic heat production of crustal rocks: An assessment based on geochemical data. Geophysical Research Letters, 14(3): 295−298. DOI：10.1029/GL014i003p00295.

Wu AM, Ma F, Wang GL, et al. 2018. A study of deep-seated karst geothermal reservoir exploration and huge capacity geothermal well parameters in Xiongan New Area. Acta Geoscientica Sinica, 39(05): 523−532. (in Chinese) DOI：10.3975/cagsb.2018.071104.

Wang YB, Liu SW, Chen CQ, et al. 2024. Compilation of terrestrial heat flow data in continental China (5th edition). Chinese Journal of Geophysics, 67(11): 4233−4265. (in Chinese) DOI：10.6038/cjg2024S0284.

Xing YF, Wang HQ, Li J, et al. 2022. Chemical field of geothermal water in Xiong'an New Area and analysis of influencing factors. Geology in China, 49(06): 1711−1722. (in Chinese) DOI：10.12029/gc20220601.

Yao YH, Jia XF, Li ST, et al. 2022. Heat flow determination of Archean strata under the karst thermal reservoir of D01 well in Xiong'an New Area. Geology in China, 49(6): 1723−1731. (in Chinese) DOI：10.12029/gc20220602.